International Communications in Heat and Mass Transfer 125 (2021) 105284

Contents lists available at ScienceDirect

International Communications in Heat and Mass Transfer

journal homepage: www.elsevier.com/locate/ichmt

Liquid film boiling on plain and structured tubular surfaces with and without hydrophobic coating

Pu-Hang Jin [a], Ibrahim Mostafa [a], Peng He [a], Zhuo Zhang [a], Chuang-Yao Zhao [b], Wen-Tao Ji [a], Wen-Quan Tao [a,*]

[a] Key Laboratory of Thermo-Fluid Science and Engineering of Ministry of Education, Xi'an Jiaotong University, Xi'an 710049, PR China
[b] School of Building Services Science and Engineering, Xi'an University of Architecture and Technology, Xi'an 710055, PR China

ARTICLE INFO

Keywords:
Liquid film boiling
Hydrophobic coating
Reentrant cavity
Low surface tension fluid

ABSTRACT

In this study, thin liquid film boiling heat transfer characteristics of R134a on a plain and two finned tubular surfaces were experimentally investigated. The dependence of heat transfer coefficient (HTC) on the composite effects of microstructure and hydrophobic coating was characterized. It is found that HTC increases monotonously with increasing heat flux until reaching a threshold heat flux (THF), beyond which the HTC starts to descend. The THF is highest for the plain surface and lowest for the boiling-enhanced surface due to the effect of reentrant cavities. The boiling-enhanced surface shows larger HTC under low heat fluxes (less than 60 kW m^{-2}) compared with the condensation-enhanced counterpart, whereas the latter one is superior when the heat flux exceeds 60 kW m^{-2}. Hydrophobic coating can substantially intensify the liquid film boiling heat transfer on boiling-enhanced finned surface with reentrant cavities. The intensification of heat transfer is more prominent in cases of high heat flux.

1. Introduction

Boiling is ubiquitous in heat dissipation devices due to its high efficiency brought out by the large latent heat of phase change [1]. The boiling heat transfer intensification is one of the dynamic research topics to meet the challenges of the cooling requirement in electronics industry, petrochemical engineering, refrigeration and power generation system, etc. [2]. In large-scale water chillers, tubular surfaces are always served as the heat transfer interface of flooded or falling-film type evaporators [3]. Taking a falling-film evaporator as an example, chilled water goes inside the tubes and refrigerant evaporates at the tubes' outside surfaces, and usually refrigerant (shell) side presents the dominant thermal resistance. An increase in shell-side heat transfer coefficient (HTC) enables a reduced size of evaporator and is favorable to increase system coefficient of performance (COP).

Among many strategies to enhance nucleate boiling heat transfer, the techniques based on surface modification, including changing surface morphology by adopting micro/nano structures, changing surface wettability by surface coatings and both [2,4–13], have obtained a great attention [1,14–17]. These modified surfaces have been shown to be conductive to improving the crucial aspects of nucleate boiling heat transfer like earlier onset of nucleate boiling (ONB), larger heat transfer coefficient (HTC) and higher critical heat flux (CHF) [18–20]. Followings are some examples reported in literature. Hydrophobic surfaces with low surface energy coatings usually provide higher HTCs but lower CHF than those of the hydrophilic ones [1,18,19]. At small wall superheat, less free energy is required for nucleation, inducing earlier ONB and larger bubble release frequency on hydrophobic surfaces [21,22]. Whereas, at larger wall superheat, coalescence of neighboring bubbles on the heated surface results in an inferior heat dissipation efficiency for the hydrophobic surfaces compared with hydrophilic ones. Superhydrophilic surface, with the apparent contact angle with water close to 0°, can increase the CHF by improving the liquid supply to nucleate sites and enhancing capillary-driven evaporation [16]. Lower boiling incipience temperature was achieved on micro-porous copper surfaces and the HTC and CHF was enhanced by50 - 270% and 33 - 60%, respectively, as compared with the plain counterpart [13]. The apparent contact angle (CA) between refrigerant and metal/silicon surface is usually close to 0°, showing an intrinsic super-philic property [23,24]. The hydrophobic coatings can hardly change the apparent CA between low surface tension fluids and solid substrate. For this reason, less attention has been given to low-surface-tension fluids like refrigerants compared with water. However, low surface energy coatings are shown to influence the

* Correspondent author.
E-mail address: wqtao@mail.xjtu.edu.cn (W.-Q. Tao).

https://doi.org/10.1016/j.icheatmasstransfer.2021.105284

Available online 30 April 2021

Nomenclature

c	Enhancement factor of internal surface
D	Diameter of tube, mm
Fpi	Fin density or fins per inch
H	Fin height, mm
h	Heat transfer coefficient / HTC, W $m^{-2}K^{-1}$
k	Enhancement factor of outer surface
L	Tube length, mm
q	Heat flux, kW m^{-2}
R	Thermal resistance, m^2K W^{-1}
Re_{Γ}	Film Reynolds number
T	Temperature, °C
U	Overall heat transfer coefficient, W $m^{-2}K^{-1--}$

Greek

Δ	Variable differential
Γ	Liquid film flow rate on one side of the tube per unit length, kg $m^{-1}s^{-1}$
μ	Dynamic viscosity, kg $m^{-1}s^{-1}$
δ	Tube wall thickness, mm

Subscript

Gni	Gnielinski equation
i	Inside of tube
o	Outside of tube
sat	Saturation
w	Wall

wetting and evaporation at thin film meniscus region though the apparent CA is hardly changed [25,26] and enhance the refrigerant condensation heat transfer in micro channels [27]. The study and application of the above-mentioned enhanced methods to the thin film boiling of refrigerants are still very limited.

Thin liquid film boiling has been shown an effective way to further enhance nucleate boiling heat transfer. Ji et al. [28,29] indicated that the HTCs of falling film evaporation with nucleate boiling are higher than those of pool boiling on the same enhanced surface in cases with low heat flux. Wang and Chen [30,31] found that the nucleate boiling can be greatly intensified when the liquid film thickness was decreased to the range from hundreds of microns to a few tens of microns. The effects of some key parameters (like surface material, roughness and microstructure, heat flux, saturation temperature, low GWP refrigerant and lubrication oil) on refrigerant liquid film boiling heat transfer have been investigated in [32–37]. However, the effects of each parameter are highly dependent on the concurrent variations of other parameters, making the heat transfer characteristics extremely puzzling, especially for enhanced surface. Commercial pool-boiling enhanced tube with open microstructures or re-entrant tunnels may enhance the thin film boiling heat transfer by extending heat transfer area, increasing nucleation site density, altering the vapor-liquid interaction behaviors within the tunnels or creating more micro-layer vaporization [3]. The interconnected cross channels may also provide extra capillary force, making the the liquid be sucked into the tunnel space, which provides better liquid replenishment to the active nucleation sites. As for the reentrant cavity, a larger cavity mouth offers a longer three-phase contact line, inducing larger heat transfer rate [21]. Given that the most commercial boiling enhanced tubes used in previous studies [28,29] are originally designed for pool boiling evaporator, some 3D integral finned condensation tubes may perform better in liquid film boiling heat transfer than the pool-boiling enhanced tubes [32].

Although numerous results have been published with mostly positive influences for water, there still is a large room to apply the surface modification techniques to low surface tension fluids. Especially, few studies have illuminated the effects of hydrophobic coatings on thin liquid film boiling heat transfer. In this case, the research focus of the present paper is paid on the HTC intensification of refrigerant thin liquid film boiling to unravel the composite effects of micro-scale structures and nano-scale coatings. The remaining part of this paper is organized as follows. Section 2 introduces the methods for surface preparation and characterization. Section 3 exhibits the experimental facilities and data reduction methods. Section 4 presents the experimental results and discussions. Finally, some conclusions are summarized in Section 5.

2. Surface preparation and characterization

Taking the falling film evaporator as an applicable candidate, three copper tubes (plain, boiling and condensation) with nominal outer diameter of 3/4 in. were used as the test samples. Both sides (internal and outside) of the plain tube (termed as P tube in following parts) are smooth, while for the boiling enhanced tube (B tube) and condensation enhanced tube (C tube), there are helical micro-fins on their inner surfaces to improve the water-side single phase convective heat transfer. Reentrant cavities and 3-D integral fins were machined on the outside of the B and C tubes, respectively. Detailed specifications of the tubes and the microstructure scanning pictures of the enhanced surfaces can be found in Table 1 and Fig. 1, respectively. It should be noted that the boiling-enhanced (B) tube is originally designed for pool-boiling and the condensation-enhanced (C) tube is commonly used for enhancing film-wise condensation. However, when applied to thin liquid film evaporation/boiling, C tube is shown to possess better heat transfer performance than B tube [32]. Apart from the specific geometries, the fin shapes of B and C tube have great differences. Fins on B tube are bent with smaller outlet width of each cavity (to create reentrant cavities) compared with that of the C tube, where micro fins are vertical to the tube wall with some pointy tip on top of them, as shown in Fig. 1.

To study the composite effects of micro-structure and hydrophobic coating on thin liquid film boiling heat transfer, the three tubes' outer surfaces were modified by low surface energy coatings. To this end, each of the three tubes were equally cut into five pieces by wire-electrode cutting. After cutting, the five pieces of each tube were numbered in order and their connection positions were carefully marked for soldering after coating. Then the sample tubes were cleaned with acetone in an ultrasonic bath for 15 min and rinsed with ethanol, isopropyl alcohol, and deionized water (DI water) in sequence. The tubes were then dried with nitrogen gas. Shieldex (Fig. 2, supplied by Integrated Surface Technologies) was used as the coating material. The coating process was performed in the plasma-assisted chemical vapor deposition (CVD) system (Integrated Surface Technologies BL200, Fig. 2) for 17 min with the chamber pressure of 200 mTorr and the electrode power of 105 W. The halocarbon gas was dissociated by plasma (76 kHz), then the generated CF_2-CF_3 polymer material was deposited onto the tubes' surfaces to form hydrophobic coatings. The thickness of the coating, based on the information given by the plasma system provider (Integrated Surface Technologies), is around 20 nm, having negligible influence on the heat conduction through the tube wall. Static water CA

Table 1
Parameters of the tested tubes (unit: mm).

	L	δ	D_i	D_o	Fpi	H
P tube	1520	1.1	16.66	19.02	/	/
B tube	1520	1.14	16.33	18.86	56	0.65
C tube	1520	1.14	16.33	18.86	50	0.66

Note: For B and C tubes, D_i and D_o are their embryo tube diameters.

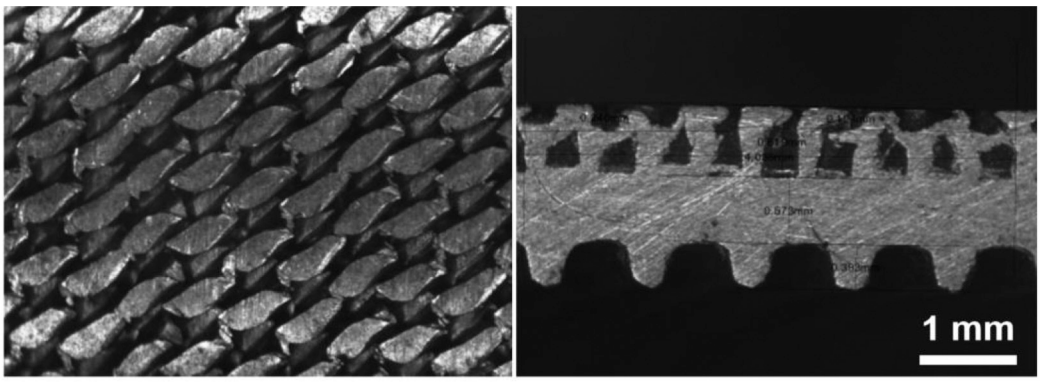

(a) Tube B (Boiling enhanced tube)

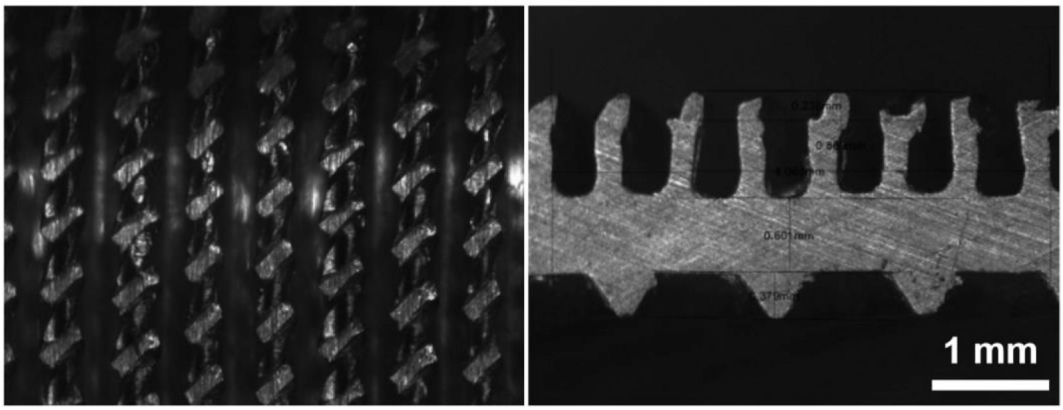

(b) Tube C (Condensation enhanced tube)

Fig. 1. Doubly enhanced structures of the boiling and condensation enhanced tubes.

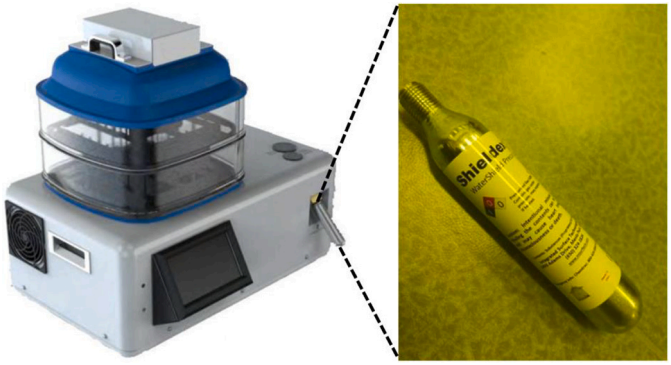

Fig. 2. The plasma system for chemical vapor deposition (CVD).

was also measured on the coated plain tube after the boiling test to check the hydrophobic coating is intact or not. It's shown that the coated surface still exhibited a repellent property to water after refrigerant boiling test. During the coating process, the two ends of the tubes were capped to avoid the coating on inner surfaces. Finally, the individual samples were connected in sequence by cold welding which ensured the minimum heat-affected zone along the tube length. The connection angle was regulated carefully to ensure the same condition as the uncoated tubes as much as possible.

Since the CA of low-boiling-point refrigerant (like R134a) should be measured at vacuum environment, high-boiling-point fluid FC72 with surface tension of 10 mN/m, similar with that of R134a (9 mN/m), is used for characterizing the variation of the contact angle with and without the hydrophobic coating. For the convenience of CA measurement, a plain copper plate was prepared with the same way as the tested tubes. Static CA between the coated copper plate and a sessile FC72 droplet (with a volume of 2.5 μl) was measured with the contact angle meter (OCAH200, Data physics, Germany) at ambient temperature. The average value of static CA was acquired by measuring 5 times at different places for the same sample. The hydrophobic coating changes the apparent static contact angle from CA = 2 ± 2° for the uncoated Cu surface to CA = 4 ± 2° for the coated surface (Fig. 3). It worth noting that for the low surface tension fluids, the CA is close to 0° and the advancing and receding CA are both very close to 0°. That is why here the static CA is taken to characterize the surface wettability. In this study only the most important parameter, CA, was measured, no further sophisticated

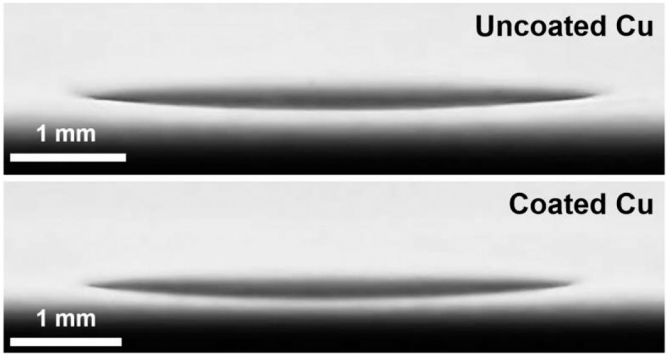

Fig. 3. Static contact angle between FC-72 droplet and the uncoated/coated copper surface.

detection such as EDS image was conducted.

It is interesting to note that hydrophobic coating will make surface more repellent. As presented above that more repellent surfaces induce an earlier ONB point and increase the HTC at low heat flux [21,22]. In this paper the maximum heat flux tested is around 150 kW m^{-2}, which is in the low heat flux regime of thin liquid boiling of refrigerant. That's why the more repellent surfaces are studied.

3. Test setup and data reduction method

3.1. Test setup

The heat transfer coefficient of thin liquid film evaporation/boiling was measured with the same test setup as that in [34]. It is comprised of three main circulations, i.e., hot water (red arrow line in Fig. 4), cold water (blue arrow line in Fig. 4) and refrigerant (black arrow line in Fig. 4) circuits, and two chambers (evaporator and condenser). The liquid film was formed by pumping liquid refrigerant in the condenser to the liquid distributor in the evaporator and spraying it onto the test tube. The falling liquid film was heated by hot water flowing inside the test tube. Temperatures of the two water tanks can be controlled by the evaporator and heaters set.

Absolute pressure in the evaporator was regarded as the saturation boiling pressure (P_{sat}) and its corresponding saturation temperature (T_{sat}) was used in calculating the temperature difference of heat transfer. Flow rates of in-tube water and liquid refrigerant were measured with electromagnetic and Coriolis flowmeter, respectively. Water inlet and outlet temperatures were detected by platinum resistance temperature detectors (RTDs). Specifications of instruments can be found in our previous work [34].

The test section was constructed in the evaporator vessel (2 in Fig. 4). Three tube positions (Fig. 5(a)) were arranged for the heat transfer test and each of them owned the same-type of liquid distributor. Each liquid distributor is comprised of a preliminary and a secondary distributor and their top-view design drawings are shown in Fig. 5(c) and (d). The tubes were fixed on two end cover flanges and the liquid distributors were fixed on the inner surface of the vessel by welding (Fig. 5(b)). The distance between tube center and bottom surface of liquid distributor is 15 mm (see Fig. 5(a)). The three secondary distributors are firstly welded on the mounting plate and then the three preliminary distributors are soldered on the secondary distributors. The diameter and pitch of the draining holes (black dots on two liquid distributor) on the bottom surfaces of the boxes are 2 mm and 10 mm, respectively. 20 venting holes are drilled on the mounting plate since the vapor outlets of the evaporator are arranged on the top of the vessel.

3.2. Test procedure

The RTDs were calibrated within the temperature range from 6 °C to 40 °C before the test. When the refrigerant was charged into the system, the heat exchange between the hot water inside the tube and the environment was examined by tests without evaporation on the tube. The environmental temperature was around 25 °C and the temperature of heating water varies from 6 °C to 40 °C, the temperature difference of inlet and outlet was within 0.03 K indicating that the test chamber and tested tube were well-insulated from the ambient environment.

During the test, the heating and chilling waters were first heated or cooled to the desired temperature. Then three pumps would circulate the water in the tubes and pump the liquid refrigerant to the liquid distributor in evaporator. For the test of a single curve, saturation temperature (T_{sat}) and film Reynolds number (Re_f) were kept constant with varied heat flux by adjusting the temperature of hot water. To make the nucleate sites on the tubes' outer surface be fully activated, the hot water was firstly heated to reach the heat flux of 70 kW m^{-2} for half an hour, then the temperature of hot water was decreased step by step until the minimum heat flux condition was reached. After this, the hot water was heated again to continue the following tests from 80 kW m^{-2} to the maximum heat flux. 10 data at each point will be saved when the deviation of saturation temperature (T_{sat}) is less than 0.03 K and heat flux within 0.3 kW m^{-2}.

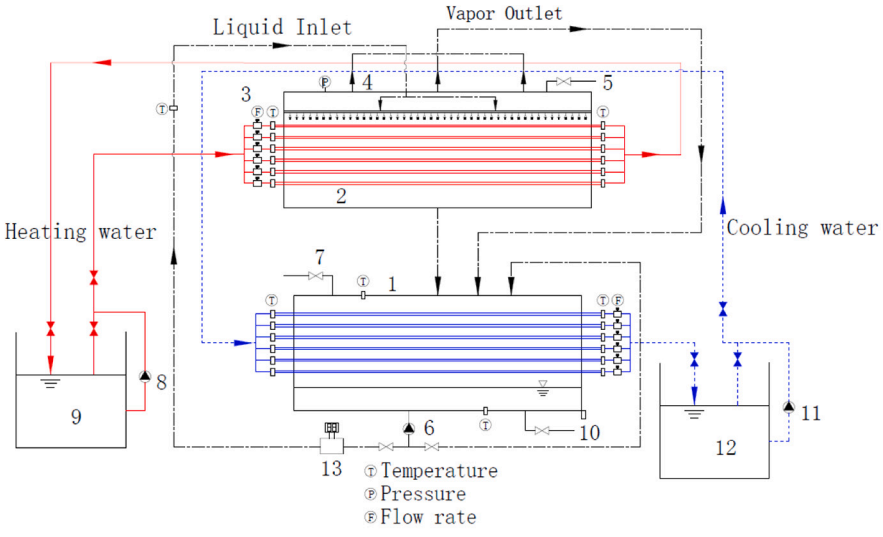

1. Condenser (reservoir); 2. Evaporator; 3. Electromagnetic flowmeter; 4. Pressure gauge; 5. Exhausting valve; 6. Refrigerant magnetic pump; 7. Refrigerant charging valve; 8. Heating water pump; 9.Hot water tank; 10. Refrigerant outlet; 11. Cooling water pump; 12. Cooling water tank; 13. Refrigerant mass flow meter.

Fig. 4. Schematic diagram of the test system.

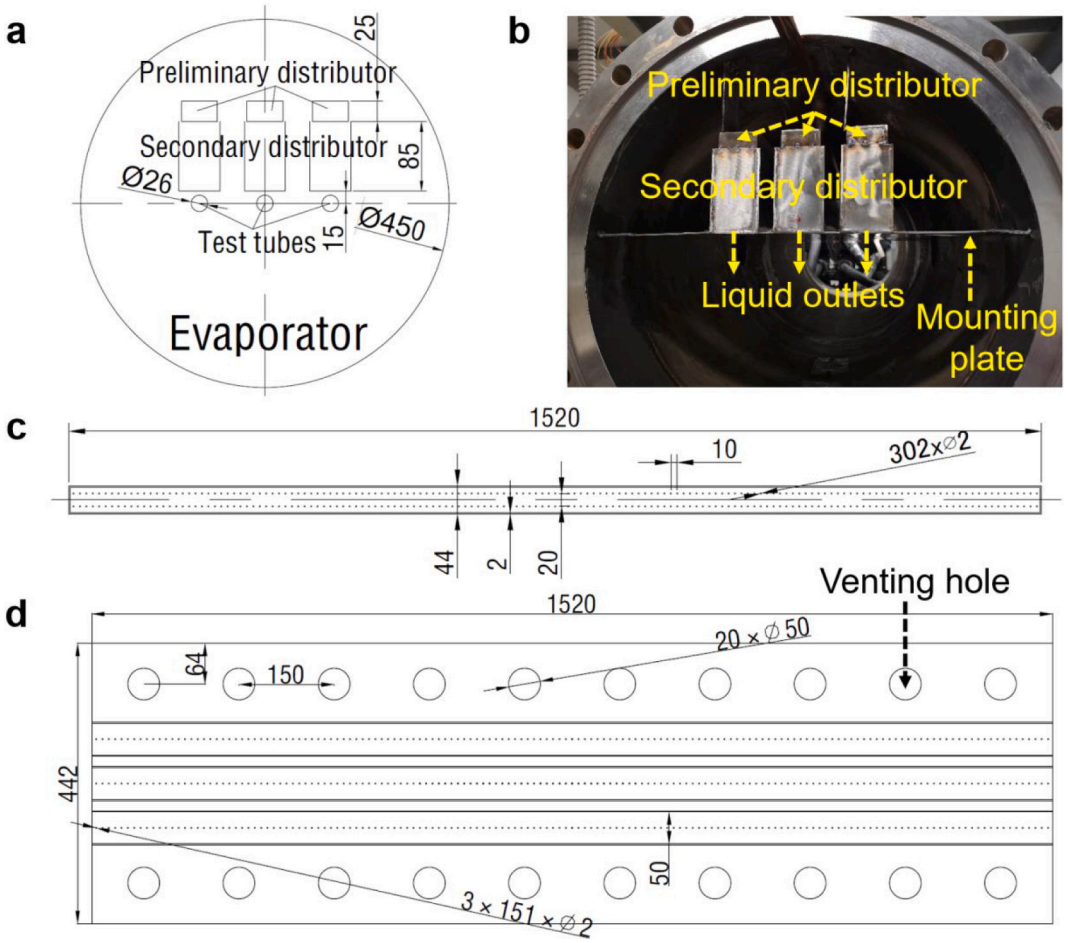

Fig. 5. Test section.

3.3. Date reduction and uncertainty analysis

To investigate the liquid film boiling heat transfer characteristics on the tube's outer surface, the area-weighted average HTC on the tube's outer surface (h_o) needs to be separated from the overall HTC (U). And h_o can be expressed by Eq. (1):

$$h_o = \left[\frac{1}{U} R_w - \frac{1}{c_i h_{Gni}} \frac{D_o}{D_i}\right]^{-1} \quad (1)$$

where R_w is the tube wall thermal resistance, h_{Gni} is the water-side convection HTC estimated by Gnielinski correlation [38,39] for smooth surface, c_i is the enhancement factor of the tube's internal surface, and D_i and D_o are the inner and outer diameters of the embryo tube, respectively.

The heat flux (q_o) in following paragraphs and figures is also an average value evaluated at the tube's outer surface and film Reynolds number (Re_Γ) is defined by Eq. (2):

$$Re_\Gamma = \frac{4\Gamma}{\mu_l} \quad (2)$$

where Γ is the film flow rate on one side of the tube per unit length and μ_l is the dynamic viscosity of liquid R134a at evaporation temperature.

To minimize the measurement uncertainty of h_o, water velocity was adjusted accordingly, making the water inlet and outlet temperature difference being no less than 1 °C. Apart from the temperature difference, the uncertainty of h_o also comes from the Gnielinski equation [38,39] employed in the calculation of inner surface convection HTC, h_i. By performing the uncertainty propagation analysis [40], results show that the maximum uncertainty of q_o and h_o ranges from 3.1% to 5.8% and from 9% to 23.7%, respectively. The more detailed data reduction method and uncertainty analysis can be found in our previous work [34].

4. Experimental results and analysis

4.1. Enhancement factor of the internal surface

Enhancement factors (c_i) of the tubes' inner surfaces were acquired by Wilson plot method [41]. As demonstrated in [42], for each tube, by calculating the slope of the fitting curve shown in Fig. 6, the value of c_i of that tube can be determined, as listed in Table 2 where B, B1, C and C1 represent the uncoated boiling tube, coated boiling tube, uncoated condensation tube and coated condensation tube, respectively. The enhancement factors of coated tubes (B1 and C1) show a little bit smaller values than those of the uncoated ones (B and C). This can be attributed to the thermal affected area by cold soldering, where some micro fins on the tube internal surfaces may deform or even be damaged.

4.2. Heat transfer characteristics of the uncoated plain, condensation-enhanced and boiling-enhanced tubes

HTC variation trends versus heat flux of the three tubes are plotted in Figs. 7(a), 7(b), and 7(c), respectively. Each tube was tested with varied heat flux under three film Reynolds numbers (Re_Γ = 500, 800, and 1600) at the constant saturation temperature of 6 °C.

For the plain tube (Fig. 7(a)), HTC increases monotonously with increase in heat flux under all film Reynolds numbers until a threshold

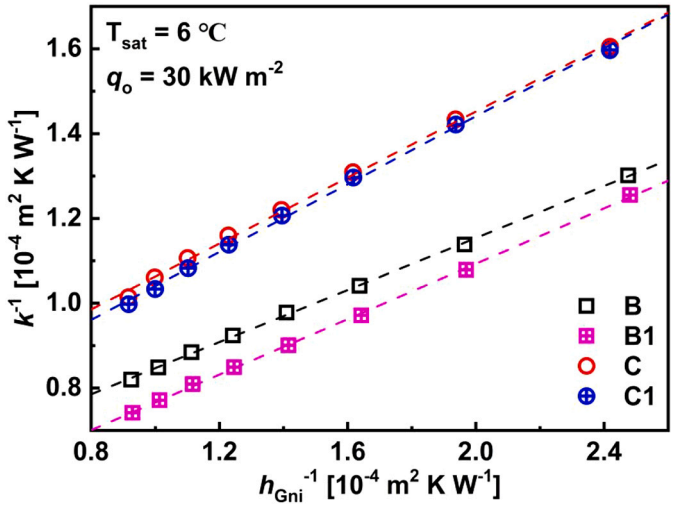

Fig. 6. Wilson plot for the calculation of internal enhancement factor of doubly-enhanced boiling and condensation tubes.

Table 2
Enhancement factors of the water-side enhanced surfaces.

Tube number	B	B1	C	C1
Enhanced factor c_i	3.20	3.10	2.90	2.85

heat flux (THF, marked by the symbols with a cross) beyond which HTC begins to decline. When q_o is lower than 40 kW m^{-2}, film Reynolds number has trivial influence on HTC. This implies that even the heat flux is less than 40 kW m^{-2}, nucleate boiling within the thin liquid film dominates the heat transfer. At higher heat fluxes (larger than 40 kW m^{-2}), the variations of HTCs exhibit following features. First, the effect of film Reynolds number becomes appreciable, and at the same heat flux the higher the film Reynolds number (Re_Γ) the larger the HTCs. Second, for the lowest film Reynolds number tested, 500, increase of HTCs with heat flux soon becomes mild and HTC reaches its maximum value at 90 kW m^{-2} (marked by the black square symbol with a cross in Fig. 7(a)). Third, for other two film Reynolds numbers, 800 and 1600, enough liquid flow rate makes the HTC further increase until the heat flux reaches 120 kW m^{-2} (red circle symbol with a cross in Fig. 7(a)) and 130 kW m^{-2}(blue triangular symbol with a cross in Fig. 7(a)), respectively. Beyond the THF points, partial dryout on the heated surface becomes more prominent with increasing heat flux and HTCs begin to decline.

The condensation enhanced surface (Fig. 7(b)) shows similar dependence of HTC on heat flux and film Reynolds number. While the THF point occurs at lower heat fluxes compared with the plain surface: THF is around 100 kW m^{-2} for C tube when $Re_\Gamma = 1600$ (130 kW m^{-2} for P tube). This is probably resulted from the extended surface area which causes a higher possibility of dryout under the same film Reynolds number as the plain surface.

For the boiling enhanced surface, the effects of heat flux and film flow rate on HTC show more or less similar characteristics as the plain and condensation-enhanced surfaces, as shown in Fig. 7(c). Nonetheless, the THF points are much smaller than those of the plain and condensation surfaces, and their values are 35 kW m^{-2}, 30 kW m^{-2} and 25 kW m^{-2} for Re_Γ = 1600, 800, and 500, respectively (marked by symbols with a cross in Fig. 7(c)). It should be noted that as far as the HTC is concerned, the HTC values of the boiling tube are much higher than those of the plain one. Within the test conditions, the maximum HTC value of the P tube is less than 13 kW m^{-2}K^{-1} while for the B tube the minimum value is larger than 14 kW m^{-2}K^{-1}.

It is interesting to compare the HTC variation trends between boiling-enhanced and condensation-enhanced surfaces, and the results

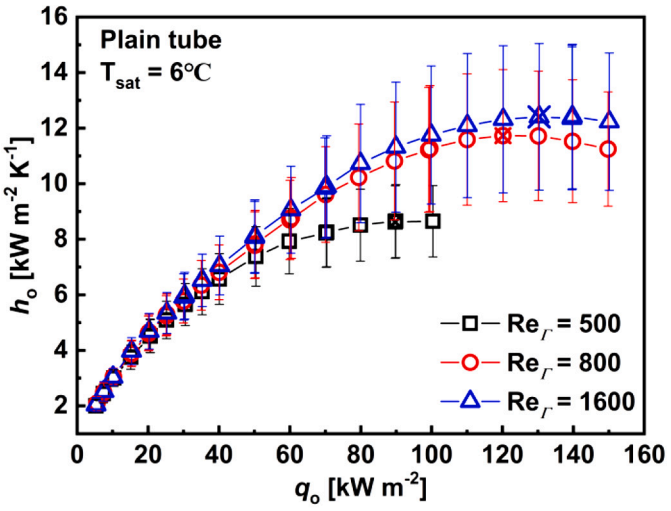

(a) Plain tube

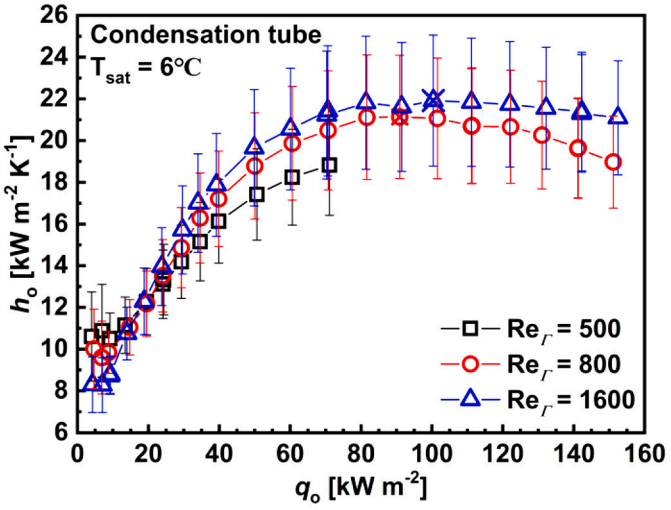

(b) Condensation tube

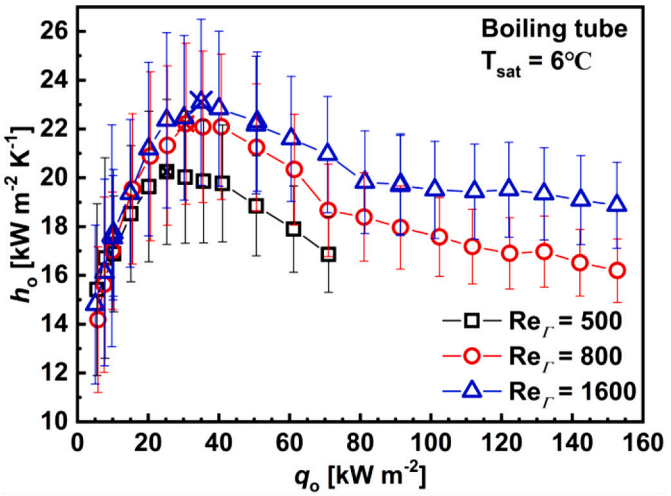

(c) Boiling tube

Fig. 7. HTC variation trend with heat flux.

are depicted in Fig. 8 for the film Reynolds number of 800. The boiling tube shows superior heat transfer performance over the condensation tube when the heat flux is lower than60 kW m^{-2}, while the trend reverses beyond this heat flux. The large differences in the HTC variation trend may be attributed to different micro-structures of the surface fin geometries. As shown in Fig. 1, the fins on the condensation-enhanced tube is straightly vertical to the tube surface, extending the heat transfer area, so that very similar HTC variation trend was observed as the plain surface. On the other hand, the reentrant cavities on boiling-enhanced tube behaved differently at low and high heat flux conditions. When the heat flux is not high, the reentrant cavities on the boiling enhanced tube can sustain the liquid and vapor seed after bubble departure which facilitate the activation of the subsequent nucleation cycle. In this way, the reentrant microcavities can enhance the wetting within the cavities and increase nucleate site density and bubble release frequency, inducing a larger HTC under lower heat fluxes. While at higher heat flux conditions, the reentrant cavities may impede the vapor escaping from the cavities because of the narrow cavity outlet, which leads to partial dryout in cavities and hence deteriorates thin liquid film boiling heat transfer behavior.

4.3. HTCs of the coated surfaces

This section shows the HTC comparison between the original surfaces (later they are termed as uncoated surfaces) and coated ones. Tests for coated surfaces were conducted with decreasing heat flux from 80 kW m^{-2} to 10 kW m^{-2} at the same saturation temperature (6 °C) as that of the uncoated surfaces. The coated plain surface shows almost identical HTC to that of the uncoated surface (Fig. 9(a)). This can easily be understood since the hydrophobic coating can only change the apparent contact angle of refrigerant R134a a little. For the open-channel 3-D integral fin surface, some discrepancy appears with slightly higher HTCs on the coated one, as shown in Fig. 9(b). However, the authors would rather to attribute it to the measurement uncertainty since the largest deviation is only 9.9%. These results indicate that the hydrophobic coating can hardly affect the nucleate boiling heat transfer for low surface tension fluids.

Intriguingly, thing changes for the boiling enhanced surface. Prominent heat transfer enhancement can be observed from Fig. 9(c). The HTC enhancement ratio ranges from 21.0% to 60.4% with respect to the uncoated tube (see Fig. 10), which is far beyond the measurement uncertainty. It should also be noted that the enhancement ratio (*k*, the ratio of falling film evaporation HTC between coated and uncoated tube)

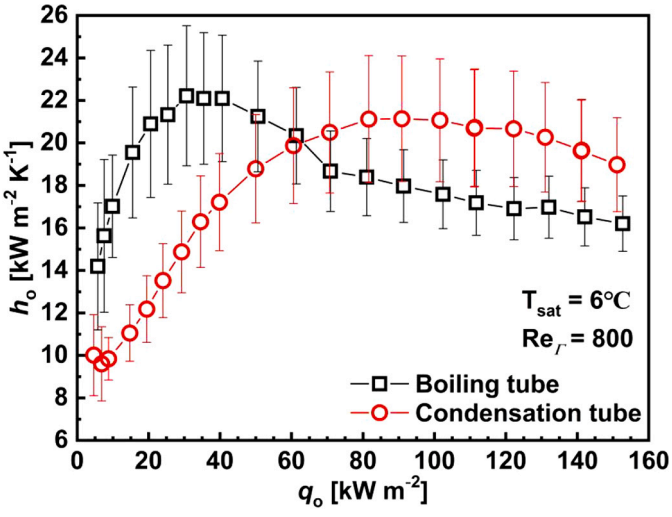

Fig. 8. HTC comparison between boiling-enhanced and condensation-enhanced tubes.

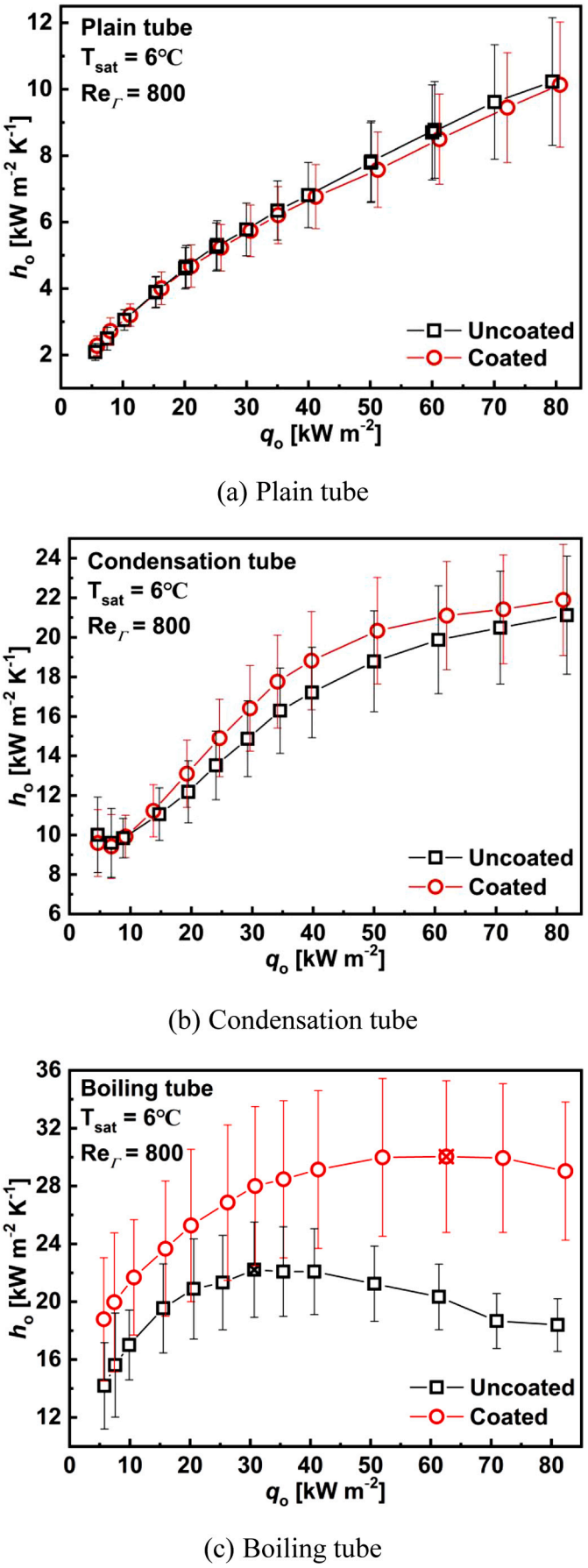

Fig. 9. Comparison of HTCs between the coated and uncoated surfaces.

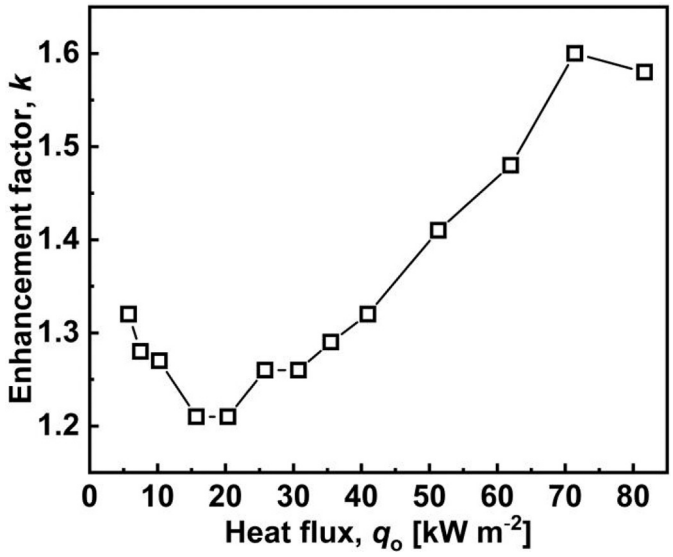

Fig. 10. Enhancement factor of the coated boiling-enhanced tube versus heat flux.

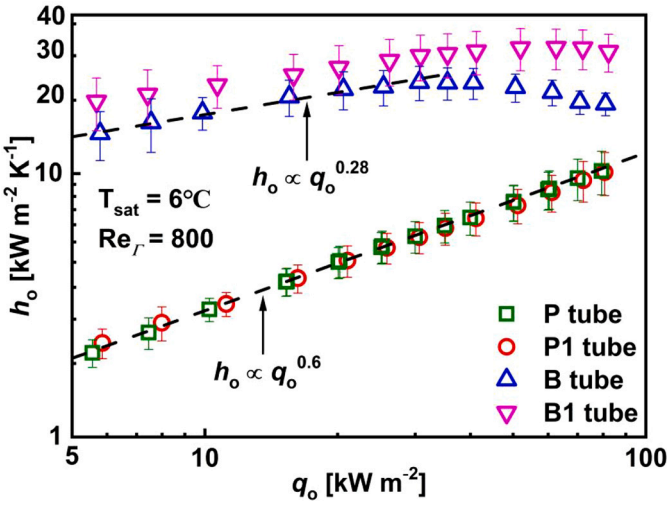

Fig. 11. HTC variation curve versus heat flux in log-log coordinate.

becomes even higher at larger heat fluxes (Fig. 10) and the THF where the maximum HTC is achieved becomes larger (60 kW m^{-2}) compared with the uncoated surface (30 kW m^{-2}) when $Re_\Gamma = 800$ (see Fig. 9(c)).

Fig. 11 shows the HTC variation trends versus heat flux in log-log coordinate of the uncoated and coated P and B tubes. Within the whole test range of heat flux for plain surface, the HTC shows an exponential relationship with the heat flux with a constant power of 0.6, which is similar to that of spraying cooling through a thin liquid film in [43] and very close to 0.67 for pool boiling curve as shown by the Cooper Eq. [44]. This indicates that for the cases studied nucleate boiling predominates the falling film evaporation heat transfer. However, for boiling enhanced surface, the exponential relationship exists only for low heat fluxes (< 30 kW m^{-2}) cases with a much smaller exponent of 0.28, even though the HTCs values are 1.43–6.8 times larger than those of the plain tube. This demonstrates that remarkable dryout is happening during phase change within reentrant microcavities not only at large heat flux regime (35 kW m^{-2} or larger) but also at very low heat fluxes (from 5 kW m^{-2} to 30 kW m^{-2}).

The intensification of thin film boiling heat transfer by the hydrophobic coating on boiling enhanced surface may be understood as follows. When bubbles are nucleated in the micro structured tunnels, they induce a two-phase channel flow in the phase of bubble growth and breakage, making the cavities being partially occupied by vapor. Within reentrant cavities, the bubble path is much more convoluted compared with the plain surface and the condensation enhanced surface, inducing more thin film meniscus region. In this case, a significant portion of the vapor needs to penetrate the narrow outlet of the reentrant cavities to escape from the cavities. In addition, the micro fins can create capillary force to enhance the liquid supply to nucleate sites. These two actions lead to two-phase flow within the micro structures of the boiling-enhanced surface studied in this paper. The hydrophobic coating with lower surface energy may reduce the friction loss of two-phase flow in microchannels created by reentrant cavities and can accelerate the vapor escaping from reentrants, thus enhancing thin film boiling heat transfer.

5. Conclusions

Thin film boiling heat transfer characteristics on a tubular plain surface and two finned surfaces were studied in this paper. The composite effects of microstructure and hydrophobic coating on HTC were studied. The main findings of this study are as follows:

1. For all three surfaces tested, HTC increases monotonously with increasing heat flux under all film Reynolds numbers until a threshold heat flux, beyond which HTC begins to decline. THF is largest for the plain surface and smallest for the boiling surface with reentrant cavities.
2. The boiling-enhanced surface exhibits superior heat transfer performance at lower heat fluxes than the condensation-enhanced surface, while the latter is more prominent in cases of higher heat fluxes.
3. Hydrophobic coating can hardly influence the liquid film boiling heat transfer on both the plain and the condensation-enhanced finned surface.
4. Hydrophobic coating substantially intensify the thin liquid boiling heat transfer on boiling-enhanced surface with reentrant cavities. The enhancement factor is larger at high heat fluxes, inducing a larger transitional heat flux where maximum HTC is achieved.

Declaration of Competing Interest

The authors declare that they have no known competing financial interests or personal relationships that could have appeared to influence the work reported in this paper.

Acknowledgement

This work was supported by the Foundation for Innovative Research Groups of the National Natural Science Foundation of China (No. 51721004) and 111 Project (B16038).

References

[1] C.G. Jothi Prakash, R. Prasanth, Enhanced boiling heat transfer by nano structured surfaces and nanofluids, Renew. Sust. Energ. Rev. 82 (2018) 4028–4043.
[2] A.K. Dewangan, A. Kumar, R. Kumar, Nucleate boiling of pure and quasi-azeotropic refrigerants from copper coated surfaces, Appl. Therm. Eng. 94 (2016) 395–403.
[3] T.S. Emery, A. Jaikumar, P. Raghupathi, et al., Dual enhancement in HTC and CHF for external tubular pool boiling - a mechanistic perspective and future directions, Int. J. Heat Mass Transf. 122 (2018) 1053–1073.
[4] K.H. Chu, Y.S. Joung, R. Enright, et al., Hierarchically structured surfaces for boiling critical heat flux enhancement, Appl. Phys. Lett. 102 (2013) 151602.
[5] H. Seo, J.H. Chu, S.Y. Kwon, et al., Pool boiling CHF of reduced graphene oxide, graphene, and SiC-coated surfaces under highly wettable FC-72, International Journal of Heat and Mass Transfer 82 (2015) 490–502.
[6] S.J. Thiagarajan, R. Yang, C. King, et al., Bubble dynamics and nucleate pool boiling heat transfer on microporous copper surfaces, International Journal of Heat and Mass Transfer 89 (2015) 1297–1315.
[7] M. Ray, S. Deb, S. Bhaumik, Pool boiling heat transfer of refrigerant R-134a on TiO_2 nano wire arrays surface, Appl. Therm. Eng. 107 (2016) 1294–1303.

[8] R. Wen, Q. Li, W. Wang, et al., Enhanced bubble nucleation and liquid rewetting for highly efficient boiling heat transfer on two-level hierarchical surfaces with patterned copper nanowire arrays, Nano Energy 38 (2017) 59–65.
[9] H.T. Phan, N. Caney, P. Marty, et al., Surface wettability control by nanocoating: the effects on pool boiling heat transfer and nucleation mechanism, Int. J. Heat Mass Transf. 52 (2009) 5459–5471.
[10] H.J. Jo, H.S. Ahn, S.H. Kang, et al., A study of nucleate boiling heat transfer on hydrophilic, hydrophobic and heterogeneous wetting surfaces, International Journal of Heat and Mass Transfer 54 (2011) 5643–5652.
[11] H.J. Jo, S.H. Kim, H. Kim, et al., Nucleate boiling performance on nano/microstructures with different wetting surfaces, Nanoscale Res. Lett. 7 (2012) 242.
[12] M. Zupančič, M. Steinbücher, P. Gregorčič, et al., Enhanced pool-boiling heat transfer on laser-made hydrophobic/superhydrophilic polydimethylsiloxane-silica patterned surfaces, Appl. Therm. Eng. 91 (2015) 288–297.
[13] J. Shi, X. Jia, D. Feng, et al., Wettability effect on pool boiling heat transfer using a multiscale copper foam surface, Int. J. Heat Mass Transf. 146 (2020) 118726.
[14] D. Attinger, C. Frankiewicz, A.R. Betz, et al., Surface engineering for phase change heat transfer: a review, MRS Energy Sustainability 1 (2014), E4.
[15] H. Cho, D. Preston, Y. Zhu, et al., Nanoengineered materials for liquid-vapour phase-change heat transfer, Nature Reviews Materials 2 (2017) 16092.
[16] C.S.S. Kumar, G.U. Kumar, M.R.M. Arenales, et al., Elucidating the mechanisms behind the boiling heat transfer enhancement using nano-structured surface coatings, Applied Thermal Engineering 137 (2018) 868–891.
[17] X. Li, I. Cole, J. Tu, A review of nucleate boiling on nanoengineered surfaces - the nanostructures, phenomena and mechanisms, Int. J. Heat Mass Transf. 141 (2019) 20–33.
[18] H. O'Hanley, C. Coyle, J. Buongiorno, et al., Separate effects of surface roughness, wettability, and porosity on the boiling critical heat flux, Appl. Phys. Lett. 103 (2013), 024102.
[19] B. Köroğlu, K.S. Lee, C. Park, Nano/micro-scale surface modifications using copper oxidation for enhancement of surface wetting and falling-film heat transfer, Int. J. Heat Mass Transf. 62 (2013) 794–804.
[20] Y.Y. Li, Z.H. Liu, B.C. Zheng, Experimental study on the saturated pool boiling heat transfer on nano-scale modification surface, Int. J. Heat Mass Transf. 84 (2015) 550–561.
[21] Y.T. Mu, L. Chen, Y.L. He, et al., Nucleate boiling performance evaluation of cavities at mesoscale level, Int. J. Heat Mass Transf. 106 (2017) 708–719.
[22] W.Z. Fang, L. Chen, Q.J. Kang, et al., Lattice Boltzmann modeling of pool boiling with large liquid-gas density ratio, Int. J. Therm. Sci. 114 (2017) 172–183.
[23] B. Vadgama, D.K. Harris, Measurements of the contact angle between R134a and both aluminum and copper surfaces, Exp. Thermal Fluid Sci. 31 (2007) 979–984.
[24] X. Lu, J. Liu, X. Xu, Contact angle measurements of pure refrigerants, Int. J. Heat Mass Transf. 102 (2016) 877–883.
[25] H. Peng, L. Lin, G. Ding, Experimental research on wetting behavior of refrigerant-oil mixture on micro/nanostructured surface, Int. J. Refrig. 62 (2016) 207–221.
[26] H. Peng, L. Lin, G. Ding, Influence of fluorinated self-assembled monolayer on wetting dynamics during evaporation of refrigerant-oil mixture on metal surface, Int. J. Refrig. 79 (2017) 76–88.
[27] Y. Ding, L. Jia, Y. Zhang, et al., Investigation on R141b convective condensation in microchannel with low surface energy coating and hierarchical nanostructures surface, Appl. Therm. Eng. 155 (2019) 480–488.
[28] W.T. Ji, C.Y. Zhao, D.C. Zhang, et al., Effect of vapor flow on the falling film evaporation of R134a outside a horizontal tube bundle, Int. J. Heat Mass Transf. 92 (2016) 1171–1181.
[29] W.T. Ji, E.T. Zhao, C.Y. Zhao, et al., Falling film evaporation and nucleate pool boiling heat transfer of R134a on the same enhanced tube, Appl. Therm. Eng. 147 (2019) 113–121.
[30] Q. Wang, R. Chen, Ultrahigh flux thin film boiling heat transfer through nanoporous membranes, Nano Lett. 18 (2018) 3096–3103.
[31] Q. Wang, R. Chen, Widely tunable thin film boiling heat transfer through nanoporous membranes, Nano Energy 54 (2018) 297–303.
[32] C.Y. Zhao, P.H. Jin, W.T. Ji, et al., Experimental investigations of R134a and R123 falling film evaporation on enhanced horizontal tube, Int. J. Refrig. 75 (2017) 190–203.
[33] P.H. Jin, C.Y. Zhao, W.T. Ji, et al., Experimental investigation of R410A and R32 falling film evaporation on horizontal enhanced tubes, Appl. Therm. Eng. 137 (2018) 739–748.
[34] P.H. Jin, Z. Zhang, I. Mostafa, et al., Heat transfer correlations of refrigerant falling film evaporation on a single horizontal smooth tube, Int. J. Heat Mass Transf. 133 (2019) 96–106.
[35] D. Jige, H. Miyata, N. Inoue, Falling film evaporation of R1234ze(E) and R245fa on a horizontal smooth tube, Exp. Thermal Fluid Sci. 105 (2019) 58–66.
[36] B.D. Bock, J.P. Meyer, J.R. Thome, Falling film boiling and pool boiling on plain circular tubes: influence of surface roughness, surface material and saturation temperature on heat transfer and dryout, Exp. Thermal Fluid Sci. 109 (2019) 109870.
[37] L.H. Chien, Y.L. Tsai, C.H. Chang, A study of pool boiling and falling-film vaporization with R-245fa/oil mixtures on horizontal tubes, Int. J. Heat Mass Transf. 133 (2019) 940–950.
[38] V. Gnielinski, New equations for heat and mass transfer in the turbulent flow in pipes and channels, Int. Chem. Eng. 16 (1976) 359–368.
[39] V. Gnielinski, On heat transfer in tubes, Int. J. Heat Mass Transf. 63 (2015) 134–140.
[40] S.J. Kline, F.A. McClintock, Describing uncertainties in single-sample experiments, Mech. Eng. 75 (1953) 3–9.
[41] S.M. Yang, W.Q. Tao, Heat Transfer, 4th ed., Higher Education Press, Beijing, China, 2006.
[42] W.T. Ji, C.Y. Zhao, D.C. Zhang, et al., Condensation of R134a outside single horizontal titanium, cupronickel (B10 and B30), stainless steel and copper tubes, Int. J. Heat Mass Transf. 77 (2014) 194–201.
[43] S.S. Hsieh, T.C. Fan, H.H. Tsai, Spray cooling characteristics of water and R-134a. Part I: nucleate boiling, Int. J. Heat Mass Transf. 47 (2004) 5703–5712.
[44] M.G. Cooper, Saturation nucleate pool boiling - a simple correlation, Int. Chem. Engng. Symp. Ser. 86 (1984) 785–792.